Elastic constant and Brillouin oscillations in sputtered vitreous SiO_2 thin films

H. Ogi,* T. Shagawa, N. Nakamura, and M. Hirao
Graduate School of Engineering Science, Osaka University, Toyonaka, Osaka 560-8531, Japan

H. Odaka and N. Kihara
Research Center, Asahi Glass Co., Ltd., Yokohama, Kanagawa 221-8755, Japan
(Received 25 June 2008; revised manuscript received 10 August 2008; published 14 October 2008)

We studied the relationship between elastic constants and microstructure in sputtered vitreous SiO_2 thin films using pump-probe picosecond laser ultrasound. The delayed probe light pulse is diffracted by the acoustic wave excited by the pump light pulse, inducing Brillouin oscillations, seen as reflectivity change in the probe pulse, whose frequency can be used to extract the sound velocity and elastic moduli. Theoretical calculations were made to explain the asymmetric response of Brillouin oscillations and to predict the possible error limit of the determined elastic constants. The thin films containing defects exhibited lower elastic constant. A micromechanics modeling was developed to evaluate defect porosity and attenuation caused by scattering was able to predict the defect size. Elastic moduli of the defect-free specimens increased with increasing sputtering power, eventually exceeding the bulk value, and correlated with phonon frequencies, indicating that the decrease in the Si-O-Si bond angle of the tetrahedral structure increased the stiffness.

DOI: 10.1103/PhysRevB.78.134204 PACS number(s): 62.20.D−, 68.35.Iv, 78.47.J−, 78.66.−w

I. INTRODUCTION

The elastic constants of solids remain as a central issue in solid-state physics because they directly reflect the interatomic bond strength for stretching and bending. They are also sensitive to the presence of defects even when their volume fraction is small; they can be used to evaluate reliability of microstructures or nanostructures.[1,2] This paper studies the relationship between elastic moduli and microstructure of sputtered vitreous silica (υ-SiO_2) thin films using picosecond ultrasound.

υ-SiO_2 is an important insulator material used for many integrated circuits. Recently, it allows development of high-frequency resonators with a Bragg reflector because of low acoustic impedance and low damping at high frequencies.[3,4] High-frequency acoustic properties of υ-SiO_2 therefore attract many researchers. Zhu *et al.*[5] studied the frequency dependence of the longitudinal-wave attenuation of υ-SiO_2 films up to 440 GHz using the picosecond pulse-echo method. Devos and co-workers[6–8] reported intensive studies on attenuation of υ-SiO_2 thin films at frequencies near 250 GHz using Brillouin oscillations excited by picosecond ultrasound. However, the behavior of elastic moduli still remains unclear. Thin films are usually compliant compared with corresponding bulk materials because of noncohesive bonds at columnar structures,[9,10] interfaces at heterogeneous phases,[1,2,11] and nanodefects.[12] This common trend is expected to apply to υ-SiO_2 films. However, Grahn *et al.*[13] reported that the longitudinal-wave velocity of a sputtered υ-SiO_2 film was about 10% larger than that of a bulk silica, and this cause remains unexplained. We thus present a systematic study for elastic moduli and microstructure in the sputtered υ-SiO_2 film.

There are three purposes in this study. First, we theoretically construct Brillouin oscillations, considering the higher-order strain effect that has been ignored so far: we show that this effect seriously affects Brillouin oscillations from silicon, resulting in an asymmetric response. Numerical simulations predict possible errors in the elastic constants determined by Brillouin oscillations. Second, we study the cause of the stiffened thin films comparing the elastic constants with the phonon frequencies of the tetrahedral structure measured by Fourier transform infrared (FT-IR) spectroscopy. Third, we study the effect of the defects on the elastic constants using micromechanics calculations for softened thin films, and present a model to evaluate volume fraction and size of the defects.

II. BRILLOUIN OSCILLATIONS

Thomsen and co-workers[14,15] first detected high-frequency coherent acoustic phonons using ultrafast pump-probe light pulses. Following their work, the picosecond ultrasound techniques were developed for the study of ultrahigh frequency acoustic properties of solids. They are classified into three methods. First is the pulse-echo method,[5,11,13,15–17] where the acoustic pulse generated by the pump light repeats reflections between the film surface and the film-substrate interface. The round-trip time and echo amplitudes were measured to determine the sound velocity and attenuation. Second is the phonon-resonance spectroscopy,[18–21] where the standing waves in nanostructures were measured to evaluate the elasticity through their resonance frequencies. Third is the Brillouin oscillation,[6–8,15,22] which arises from interference between the light reflected at the specimen and the light refracted by the acoustic wave propagating in the transparent or translucent material. In the first-order approximation for strain, the oscillation frequency f relates with the sound velocity υ via (Bragg's condition)

$$f = \frac{2n\upsilon}{\lambda}, \tag{1}$$

when the probe light enters the film perpendicularly. Here, n and λ denote the refractive index of the examined material

 ©2008 The American Physical Society

and the wavelength of the probe light, respectively. Thus, the sound velocity is obtained by measuring the Brillouin-oscillation frequency when the refractive index is known.

Thomsen *et al.*[15] established theoretical models for the sound-wave generation and detection by the pulse light. Following their work, we calculate the reflectivity change for the v-SiO_2 films on monocrystal (001) Si substrate. We take the z axis toward the film depth. The reflection coefficient without the strain pulse is given by

$$r_0 = \frac{r_{01} + r_{12}e^{-2ik_1 d}}{1 + r_{01}r_{12}e^{-2ik_1 d}}. \tag{2}$$

Here, d is the film thickness, and r_{01} and r_{12} are reflectivity coefficients from vacuum to v-SiO_2 film and from v-SiO_2 film to the Si substrate, respectively. k_1 denotes the wave number of the probe light in the v-SiO_2 film. When an acoustic pulse is launched from the surface area and propagates in the thickness direction, the strain η changes the dielectric constants and diffracts the probe light, resulting in the change in the reflection coefficient r, which is $r=r_0+\Delta r_1+\Delta r_2$. Δr_1 and Δr_2 are the reflectivity changes caused in the v-SiO_2 film and in the Si substrate, respectively, and they are expressed by

$$\Delta r_1 = F_1(d)\int_0^d \{e^{-2ik_1 z}(1 + r_{12}e^{-2ik_1(d-z)})^2 p_1 \eta\}dz, \tag{3}$$

$$\Delta r_2 = F_2(d)\int_d^\infty \{e^{-2ik_2 z}p_2 \eta\}dz. \tag{4}$$

Here, $p_1=(\partial\epsilon_1/\partial\eta)/\epsilon_0$ and $p_2=(\partial\epsilon_2/\partial\eta)/\epsilon_0$ correspond to the piezo-optic constants of the v-SiO_2 film and Si, respectively (ϵ_0 denotes the dielectric constant in vacuum). Importantly, the sensitivity weights F_1 and F_2 depend on the film thickness d as

$$F_1(d) = -\frac{ik_0^2}{2k_1}\frac{t_{01}t_{10}}{1 + r_{01}r_{12}e^{-2ik_1 d}}, \tag{5}$$

$$F_2(d) = -\frac{ik_0^2}{2k_2}(1 + r_0)(1 - r_{12}^2)e^{-ik_1 d}e^{ik_2 d}. \tag{6}$$

We have derived these equations by summing up all possible reflections with respect to the first-order terms about the thin layer region dz and the dielectric constant change $d\epsilon$. The detectable reflectivity change is therefore calculated by

$$\Delta R = |r_0 + \Delta r_1 + \Delta r_2|^2 - |r_0|^2, \tag{7}$$

which mainly consists of the linear terms of the strain but includes the second-order terms as well. The previous work neglected the latter by assuming $\Delta R \cong 2\,\mathrm{Re}(r_0^*\Delta r_1) + 2\,\mathrm{Re}(r_0^*\Delta r_2)$. The second-order terms are, however, essential in explaining the asymmetric Brillouin oscillations from the Si substrate because of much larger piezo-optic constant as shown later.

The strain pulse generated near the surface region via the thermal expansion takes the form of[15]

$$\eta(t,z) = -\eta_0 e^{-\alpha z}e^{\{-|z-vt|/\zeta\}}\mathrm{sgn}(z - vt). \tag{8}$$

η_0 is a positive constant and ζ indicates the pulse width. The terms for pulse distortion in the surface region[15] were neglected here because they decay quickly and fail to contribute to Brillouin oscillations. We have assumed the frequency dependence of the attenuation coefficient α as

$$\alpha(\omega) = \beta\omega^2 + \gamma\omega^4. \tag{9}$$

The ω^2 term represents the absorption loss caused by the phonon-phonon relaxation process (Akhieser's relationship),[23] and the ω^4 term indicates the scattering loss by defects.

We involved the frequency-dependent attenuation effect in the strain pulse by lowering the amplitudes of the Fourier components of η at a propagation time using the attenuation values. Then, the inverse Fourier transform was used to reconstruct the strain pulse at the propagation time.

The stress and displacement continuity at the film-substrate interface and at the film surface determined phases and amplitudes of reflected and transmitted strain pulses. An example of the numerical simulation showing the relationship between the strain pulse and the reflectivity change is seen in the movie of the supplemental file.[24]

III. EXPERIMENTS

We deposited silica thin films on the (001) surface of the Si substrate using a dc sputtering method. The target was Si and the gas was a mixture of Ar and O_2. The sputtering parameters (pressure: 0.45 or 1.3 Pa, dc voltage: 130–190 V, substrate temperature: 25 or 300 °C, and so on) were varied to develop various microstructures (11 kinds of specimens). The sputtering rate was 0.5–8 Å/s. The thickness was between 420 and 1200 nm. Several specimens were simultaneously deposited at each deposition condition, and they were used for the cross-section observation by the field-emission electron microscopy (SEM), the x-ray diffraction (XRD) measurement, the refractive-index measurement by the ellipsometry, the phonon-frequency measurement by FT-IR, and the acoustic measurement by the picosecond ultrasound. The specimens for the acoustic measurement were further subjected to the deposition process to cover them with a 10 nm Al thin film as a transducer material of the acoustic pulse.

We used a mode-locking titanium-sapphire pulse laser with 100 fs pulse width, 0.7 W power, 80 MHz repetition frequency, and 800 nm wavelength. The light pulse was split into two pulses. One was used as the pump light and focused on the aluminum film to generate the acoustic pulse through thermal expansion. The other was frequency doubled (400 nm wavelength) and entered the specimen as the probe light to detect Brillouin oscillations. Both pump and probe light pulses were perpendicularly focused on the specimen surface, and their beam-spot diameters were near 30 μm. We changed the delay time of the pump light to the probe light by changing the path length of the pumping light. Details of our optics appear elsewhere.[19,20]

We measured the refractive index n by the ellipsometry for thin films:[25] the ellipsometric angle[26] was measured as a

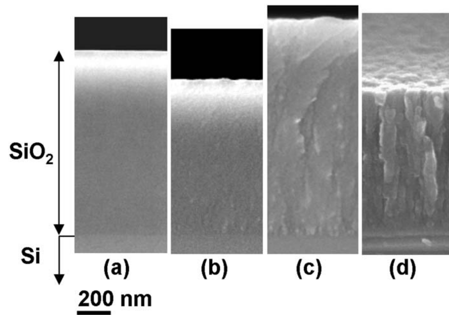

FIG. 1. Cross-section microstructures of sputtered υ-SiO_2 films: (a) S6, (b) R5, (c) R3, and (d) R1. The other smooth specimens S1–S5 showed identical microstructure to S6.

function of the wavelength between 380 and 1700 nm, and the Lorentz-oscillation model[27] was used to fit the parameters, including the film thickness as well as those needed for calculating the refractive index. Three independent measurements were done for three incident angles of 60°, 70°, and 75° for each specimen, and those results were together used in the fitting calculation. The single Lorentz oscillator in υ-SiO_2 provided successful fitting results. Because the magnitude of the imaginary part of the determined refractive index was much smaller (~0.04%) than that of the real part, we considered only the real part.

The FT-IR measurements were carried out for the wave number between 500 and 2000 cm^{-1} with the step of 2 cm^{-1}. The absorbance spectrum showed peaks near 820 and 1060 cm^{-1}, which are called ω_3 and ω_4 peaks, respectively.

The Brillouin-oscillation signal in the film was extracted from the reflectivity response, and after the background was subtracted using low-order polynomial functions, its fast Fourier transform (FFT) spectrum was calculated to determine the Brillouin-oscillation frequency f. The sound velocity and the longitudinal-wave elastic constant C_L were then determined.

IV. RESULTS

A. Microstructure of specimens

For all the specimens, the XRD spectrum showed a broad halo peak without any crystallographic peaks except for the (004)Si peak, confirming that all deposited thin films showed the amorphous phase.

Six specimens deposited at the lower pressure (0.45 Pa) with lower sputtering rates ($\leq$5 Å/s) showed very smooth microstructures as seen in Fig. 1(a); we cannot discern them from the SEM observation. Hence, we name these specimens the smooth specimens, S1–S6. Other five specimens deposited at the higher pressure (1.3 Pa) and larger sputtering rates ($\geq$4 Å/s) showed rough (granular) microstructures [Figs. 1(b)–1(d)]. We name them the rough specimens, R1–R5.

There was no correlation between the refractive index n_1 in the υ-SiO_2 film and the microstructure. The values of n_1 were between 1.46 and 1.48, and the standard deviation was less than 1%.

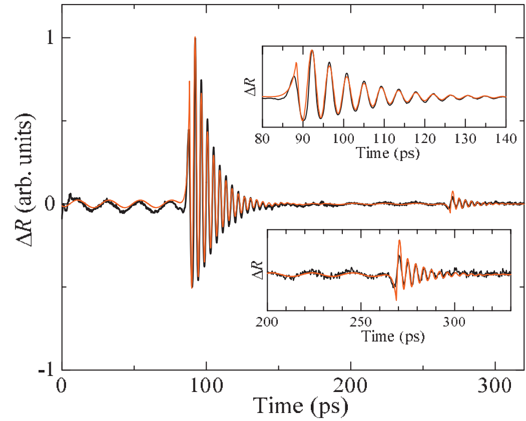

FIG. 2. (Color) Typical reflectivity change (black line) measured by the pump-probe method. The red line shows the theoretical calculation, where p_1 and η_0 were adjusted (γ=0). Inlets enlarge the high-frequency Brillouin oscillations from Si that were caused by the first strain pulse, and the pulse reflected at the interface and then at the surface.

B. Reflectivity response

The black line in Fig. 2 shows a typical reflectivity measurement for a smooth specimen. It consists of the low-frequency and high-frequency Brillouin oscillations from the υ-SiO_2 film and Si substrate, respectively. The frequency from Si was 235 GHz, which well agrees with the prediction by Eq. (1) for Si (n_2=5.57 at λ=400 nm and v_2=8437 m/s). We note that the Brillouin oscillation from Si is asymmetric about the ΔR=0 line.

The Brillouin oscillation from the υ-SiO_2 film was used to determine its elastic constant $C_L(=\rho v_1^2)$ using Eq. (1) with the measured refractivity index and the mass density of ρ=2220 kg/m^3. (The mass density could be dependent on the microstructure but, considering the insignificant variation in the refractive index, its variation will be insignificant because the refractive index correlates with the mass density.) Figure 3 shows the relationship between the sputtering voltage and the elastic constant. The elastic constant of the smooth specimens varies by more than 8% despite the fact that we cannot distinguish them from the SEM images. Important observation is that C_L of the smooth specimen shows

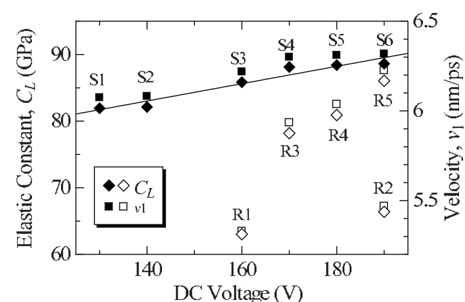

FIG. 3. The sputtered voltage versus the longitudinal-wave elastic constant C_L and the longitudinal-wave velocity v_1 of υ-SiO_2 films. The sputtering pressure was 0.45 Pa for S1–S6 and 1.3 Pa for R1–R5. The substrate temperature during the sputtering was 25 °C for S1–S6 and R3–R5, and it was 300 °C for R1 and R2.

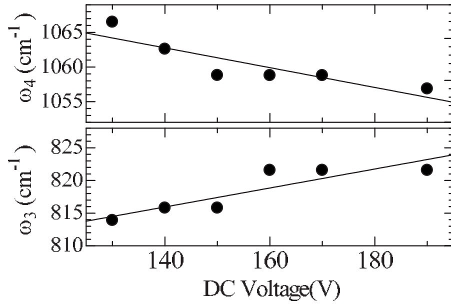

FIG. 4. Correlations between the sputtered voltage and two principal phonon frequencies [ω_4(TO) and ω_3] of the tetrahedral structure of the silica glass.

correlations with the phonon frequencies measured by FT-IR as shown in Fig. 4.

Figure 5 shows the measured reflectivity responses for the rough specimens by black lines. We observed Brillouin oscillations from v-SiO_2 for all specimens but failed to find that from Si, except for R5, which shows nearly smooth microstructure [Fig. 1(b)]. The elastic constants of the rough specimens are considerably smaller than those of smooth specimens (Fig. 3). C_L of R2, for example, is smaller than that of S6 by ~30% despite that they were deposited under the same dc voltage.

V. DISCUSSION

A. Numerical simulation

First, we investigate effects of the optical and acoustical parameters on the reflectivity response and discuss the reliability of the elastic-constant measurement using Brillouin oscillation. Equations (2)–(9) allow us to calculate the reflectivity change ΔR as a function of time. Parameters affecting ΔR are the strain-pulse width ζ, piezo-optical constants p_1 and p_2, attenuation parameters β and γ, and the initial strain amplitude η_0. The β value was fixed to be 0.9×10^{-3} nm^{-1} THz^{-2}, which led to favorable agreement between calculations and measurements. (This value is close to the reported value of 1.3×10^{-3} nm^{-1} THz^{-2} for an amorphous SiO_2 film.[7]) We used the piezo-optic constant $p_2 = -83i$ for Si, referring to Etchegoin *et al.*[28] (We extracted P_{12} value at 400 nm in Fig. 2 in Ref. 28.) It is difficult to evaluate the accurate ζ value. However, the strain-pulse shape or the ζ value will be the same because we have deposited Al thin films using the same deposition condition for all specimens. We then assumed a constant value for ζ to be 10 nm. (The ζ value dominates the frequency dependence of the strain and its variation is apparently involved in the ratio p_1/p_2.) Thus, we selected p_1 and η_0 as dominant fitting parameters, and adjusted them to fit calculations to measurements. The attenuation parameter γ was considered to simulate the measurements of the rough specimens.

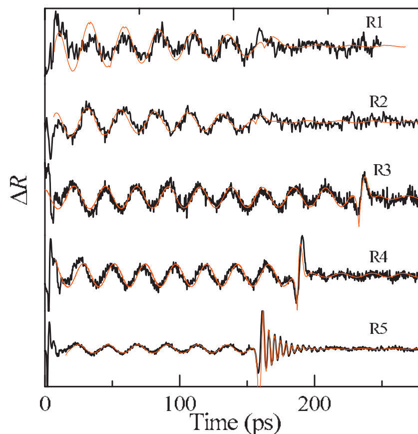

FIG. 5. (Color) Reflectivity changes measured by the pump-probe method (black lines) and those calculated by adjusting the scattering-attenuation factor γ.

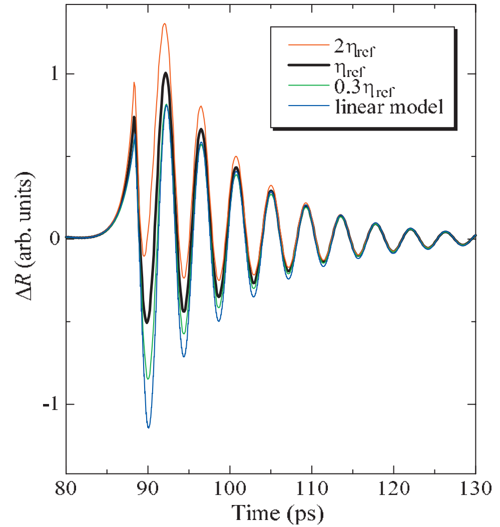

FIG. 6. (Color) Brillouin oscillation in Si calculated for the specimen in Fig. 2. The black line is the best fitted result to the measurement, and its pulse amplitude η_0 was denoted by η_{ref} to relatively investigate the effect of the pulse amplitude on the asymmetric response. The linear model means the conventional calculation, neglecting the higher-order strain contribution.

Figure 2 compares measured and calculated reflectivity changes for a smooth specimen; they show good agreement for the entire time range. The fitted parameters were $p_1 = 0.138$ and $\eta_0 = 8.2\times 10^{-12}$; the latter is a reasonable value considering the pulse-generation model proposed by Thomsen *et al.*[15] (Because of the ambiguity of ζ, the absolute value of p_1 includes the ambiguity as well, which affects the amplitude of the Brillouin oscillation in the v-SiO_2 region.)

Such a good agreement was achieved by considering the second-order terms of strain, which were neglected in the previous work. The magnitude of the Brillouin oscillation highly depends on the ambiguous parameters. However, its asymmetric response is significantly affected by the higher-order strain contribution. We numerically calculated the reflectivity change in Eq. (7) so as to fully incorporate the nonlinearity effect of the strain. Figure 6 shows Brillouin-oscillation responses in Si calculated for various initial strain amplitudes. A large strain amplitude causes asymmetric response more remarkably. Such a biasing shift represents the typical nonlinear effect. Thus, this aspect will be important for evaluating the attenuation behavior of the transparent film using the Brillouin oscillation in Si.[7]

Also, the thickness dependence of the sensitivity functions F_1 and F_2 affects the strength of Brillouin oscillations. They are dependent on the film thickness d with the period factor $2k_1$. The minimum and maximum values of $|F_2|$, for example, differ from each other by a factor of five. Thus, when the Brillouin-oscillation amplitude is used for characterization of thin films, these effects have to be taken into account for accurate evaluation.

We made many theoretical simulations for various parameters of the material (d=200–1200 nm, ζ=1–50 nm, γ=0.0005–0.01), determined the elastic constants from the FFT spectra of the calculated reflectivity changes, and compared them with the input (accurate) value. This procedure confirmed that Eq. (1) is well applicable to the determination of the elastic constant of the thin films: most cases provided the stiffness within the error of 0.5%. The largest error occurred for smaller thickness case: a 10% error for 200 nm film, for example. Our specimens are, however, thicker than 400 nm, for which the estimated error limit was less than 1%.

B. Stiffened films

The longitudinal-wave velocity of a fused silica is reported to be v_1=5850–5970 m/s (Refs. 29 and 30) at room temperature. Our results for the smooth specimens significantly exceed the standard velocity value by up to 8%. Grahn *et al.*[13] also reported the higher sound velocity of an rf-reactive sputtered silica film by 10%. Thus, v-SiO_2 films deposited by a reactive sputtering can be stiffened.

There are two possible factors for the elastic-constant increase. First is the increase in the bond strength for stretching between Si-O atoms due to the change in the interatomic distance caused by the residual stresses. Possibly, the compressive residual stress may occur because of the difference of thermal expansion with the substrate or enhanced diffusion of sputtered particles at the surface along the island particles on the substrate.[31] A compressive stress causes the enhanced stiffness through the anharmonic interatomic potential.[19] Second is the change in the tetrahedral structure; higher dc voltage for sputtering causes particles with larger energy, which can cause distortion in the tetrahedral structure.

To research these possibilities, we investigated the phonon frequencies of the thin films (Fig. 4). Vibrational modes in tetrahedral glasses including v-SiO_2 were studied by Sen and Thorpe.[32] They derived frequencies of four principal vibrational modes, assuming only the Si-O stretching bond constant C:

$$\omega_1^2 = \frac{C}{m_O}(1+\cos\theta), \tag{10}$$

$$\omega_2^2 = \frac{C}{m_O}(1-\cos\theta), \tag{11}$$

$$\omega_3^2 = \frac{C}{m_O}(1+\cos\theta) + \frac{4C}{3m_{Si}}, \tag{12}$$

$$\omega_4^2 = \frac{C}{m_O}(1-\cos\theta) + \frac{4C}{3m_{Si}}. \tag{13}$$

Here, m_O and m_{Si} are the masses of oxygen and silicon atoms, respectively, and θ denotes the Si-O-Si bridging bond angle ($\theta > \pi/2$). These results agreed with Raman spectroscopy,[33] and they were used for characterization of the bond configuration in the tetrahedral structure.

Equations (10)–(13) indicate that an increase in the stiffness for the bond stretching C increases the four principal vibrational frequencies. However, this contradicts the results in Fig. 4, where ω_3 and ω_4 show the opposite dependences on the dc voltage. Thus, the change in the elastic constant of the v-SiO_2 films is caused by the change in the bridging angle: a decrease in θ increases ω_1 and ω_3 but decreases ω_2 and ω_4, and these trends agree with the results in Fig. 4.

Therefore, the elastic constants of the v-SiO_2 films increase because of the decrease in the bridging angle. Independent studies showed that θ in v-SiO_2 decreases as the temperature increases[34] and that the sound velocity increases with the temperature increase.[30,35] These studies imply a negative correlation between θ and the stiffness in v-SiO_2, ensuring our results.

The reason why higher dc sputtering power decreases the bridging angle is possibly attributed to reduction in the average ring size of the tetrahedral structures due to higher-energy sputtering particles. Awazu *et al.*[36] reported significant decrease in θ during the heavy-ion bombardment for v-SiO_2 and attributed the cause to the reduction in the number of the membered-ring size. The transformation of the six membered rings to planar three and four membered rings will cause higher average stiffness.

C. Softened films

Because the rough specimens R1–R5 were deposited with higher dc voltage ($\geq$160 V), we expect that their intrinsic elastic constants are as large as those of specimens S3–S6. However, they show granular structures and their stiffness is significantly smaller than that of the smooth specimens (Fig. 3). Furthermore, Brillouin oscillation from Si was not observed in specimens R1–R4, indicating that high-frequency components of the strain pulse were attenuated within the v-SiO_2 film (note that Brillouin oscillation in Si is caused by the 235 GHz frequency component of strain).

The granular structure infers presence of defects, resulting in the decrease in the macroscopic elastic constant and the increase in attenuation. Here, we present a model to estimate their volume fraction and size, using a micromechanics modeling and the attenuation coefficient, assuming spherical cavities as defects.

The macroscopic elastic constants of a composite material, consisting of an isotropic matrix and inclusions, can be expressed by[37]

$$\mathbf{C}_{comp} = \mathbf{C}_M + V_f(\mathbf{C}_I - \mathbf{C}_M)\mathbf{A}. \tag{14}$$

Here, $\mathbf{C}_M$ and $\mathbf{C}_I$ are the elastic-stiffness tensors of the matrix v-SiO_2 and the defect inclusion, respectively. V_f is the volume fraction of the inclusion (porosity for the defect in-

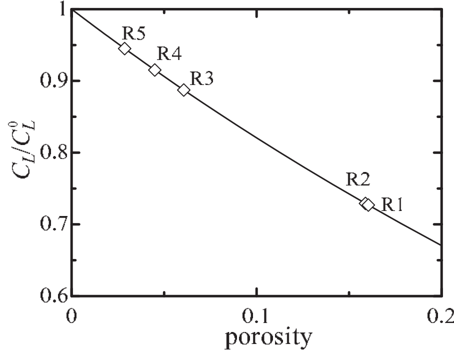

FIG. 7. The normalized decrease in the elastic constant caused by the spherical defect inclusions calculated by the micromechanics modeling (solid line). The diamond marks are the decrements of the rough specimens, from which the corresponding porosity was determined.

clusion). $\mathbf{A}$ is the strain concentration factor, and it is calculated by the Mori-Tanaka mean-field theory[38]

$$\mathbf{A} = \mathbf{A}_D[(1 - V_f)\mathbf{I} + V_f\mathbf{A}_D]^{-1}, \tag{15}$$

$$\mathbf{A}_D = [\mathbf{I} + \mathbf{S}\mathbf{C}_I^{-1}(\mathbf{C}_I - \mathbf{C}_M)]^{-1}. \tag{16}$$

These tensors are analytically calculated using Eshelby's equivalent-inclusion method.[39] $\mathbf{S}$ denotes the Eshelby tensor, and its components are simple functions of Poisson's ratio of the matrix and the shape of the inclusion. In the case of a spherical inclusion, the nonzero components of $\mathbf{S}$ are summarized in Mura's monograph.[37]

The solid line in Fig. 7 shows the dependence of the decrement of C_L on the porosity calculated using Eqs. (14)–(16). We estimated the porosity of the rough specimens so as to fit their fractional stiffness decrements to the micromechanics calculations (Fig. 7): the stiffness decrement was determined from the stiffness of the smooth specimen sputtered by the same dc voltage as the defect-free value. (In the micromechanics calculation, the elastic constants of the matrix and the inclusion used were $C_{M11}=79$ GPa and $C_{M44}=31$ GPa, and $C_{I11}=0.14$ MPa and $C_{I44}=0$. Because the fractional decrement of the stiffness was nearly independent of the matrix elastic constants $\mathbf{C}_M$, we used the standard values of the bulk υ-SiO_2 for $\mathbf{C}_M$.)

Next, we estimate the average defect size using the attenuation coefficient. While all the smooth specimens S1–S6 showed the large-amplitude Brillouin oscillation from Si, the rough specimens R1–R4 failed to show it, indicating significant scattering loss due to the defects. When the defects are spherical cavities with radius a and porosity V_f, γ is given by[40]

$$\gamma = \frac{g_c}{6v_1^4}V_f a^3. \tag{17}$$

Where g_c depends only on the velocity ratio between the longitudinal and shear waves. It nearly equals 7.3 for υ-SiO_2. We fitted the theoretical simulation of the reflectivity change to the measurement, adjusting the γ value as well as p_1 and η_0. The calculated reflectivity changes are shown by red

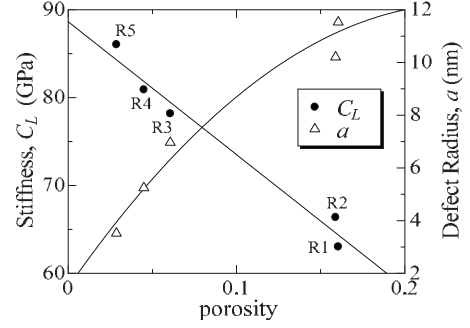

FIG. 8. Correlation among the elastic constant, porosity, and the defect radius.

lines in Fig. 5; they agree well with the measurements. Using the porosity determined by the micromechanics calculation and the fitted γ value, we determined the average defect radius a, which is shown in Fig. 8: the defect radius was estimated to be between 3.5 and 11.5 nm. Figure 9 shows the simulated strain pulses at the film-Si interface and their Fourier spectra. The strain pulse becomes broader as the porosity and defect size increase, and the 235 GHz component is negligible for the specimens R1–R4, explaining invisible Brillouin oscillation from the Si substrate.

VI. CONCLUSION

We have systematically studied elastic moduli of sputtered υ-SiO_2 thin films using Brillouin oscillations and achieved four principal conclusions. (1) The theoretical calculation demonstrated the significant contribution of the second-order strain component to the Brillouin oscillation in Si: A large strain pulse can cause the asymmetric response. (2) The theoretical calculation revealed that the Brillouin oscillation yields the elastic constant within 1% error when the film thickness is larger than 400 nm. (3) The defect-free υ-SiO_2 thin films showed larger elastic constant than the bulk value by up to 13%. The elastic constant showed correlations with the phonon frequencies of the tetrahedron structure of

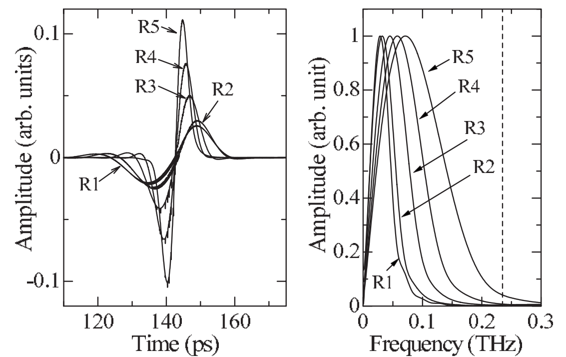

FIG. 9. Shapes of the strain pulses at the film-Si interface calculated for the rough specimens in Fig. 5 (left) and corresponding Fourier spectra (right). The middle zero-strain time was shifted so as to fit it to the result of R5 in the left figure. The dashed vertical line in the right figure shows the 235 GHz frequency, at which the Brillouin oscillation occurs in Si.

the SiO_4 unit. This trend was explained by the decrease in the Si-O-Si bridging angle and the reduction in the membered-ring size was suggested for the stiffened structure. (4) The υ-SiO_2 thin films including defects showed smaller elastic constant by $\sim$25%. We have developed a model to estimate the porosity and size of the defects. The micromechanics modeling estimated their porosity from the decrement of the elastic constant, and the scattering factor evaluated their size. The porosity was 0.03–0.16 and the defect radius was 3.5–11.5 nm.

*ogi@me.es.osaka-u.ac.jp

[1] H. Ogi, N. Nakamura, H. Tanei, R. Ikeda, M. Hirao, and M. Takemoto, Appl. Phys. Lett. **86**, 231904 (2005).

[2] H. Tanei, N. Nakamura, H. Ogi, M. Hirao, and R. Ikeda, Phys. Rev. Lett. **100**, 016804 (2008).

[3] S. Rabaste, J. Bellessa, A. Brioudea, C. Bovier, J. C. Plenet, R. Breniera, O. Marty, J. Mugnier, and J. Dumas, Thin Solid Films **416**, 242 (2002).

[4] S. Rey-Mermet, R. Lanz, and P. Muralt, Sens. Actuators B **114**, 681 (2006).

[5] T. C. Zhu, H. J. Maris, and J. Tauc, Phys. Rev. B **44**, 4281 (1991).

[6] A. Devos and R. Côte, Phys. Rev. B **70**, 125208 (2004).

[7] P. Emery and A. Devos, Appl. Phys. Lett. **89**, 191904 (2006).

[8] A. Devos, M. Foret, S. Ayrinhac, P. Emery, and B. Rufflé, Phys. Rev. B **77**, 100201(R) (2008).

[9] H. Huang and F. Spaepen, Acta Mater. **48**, 3261 (2000).

[10] N. Nakamura, H. Ogi, and M. Hirao, Acta Mater. **52**, 765 (2004).

[11] N. Nakamura, H. Ogi, T. Yasui, M. Fujii, and M. Hirao, Phys. Rev. Lett. **99**, 035502 (2007).

[12] H. Ogi, G. Shimoike, M. Hirao, K. Takashima, and Y. Higo, J. Appl. Phys. **91**, 4857 (2002).

[13] H. T. Grahn, H. J. Maris, J. Tauc, and K. S. Hatton, Appl. Phys. Lett. **53**, 2281 (1988).

[14] C. Thomsen, J. Strait, Z. Vardeny, H. J. Maris, J. Tauc, and J. J. Hauser, Phys. Rev. Lett. **53**, 989 (1984).

[15] C. Thomsen, H. T. Grahn, H. J. Maris, and J. Tauc, Phys. Rev. B **34**, 4129 (1986).

[16] O. B. Wright, B. Perrin, O. Matsuda, and V. E. Gusev, Phys. Rev. B **64**, 081202(R) (2001).

[17] A. Devos and C. Lerouge, Phys. Rev. Lett. **86**, 2669 (2001).

[18] G. A. Antonelli, H. J. Maris, S. G. Malhotra, and J. M. E. Harper, J. Appl. Phys. **91**, 3261 (2002).

[19] H. Ogi, M. Fujii, N. Nakamura, T. Yasui, and M. Hirao, Phys. Rev. Lett. **98**, 195503 (2007).

[20] H. Ogi, M. Fujii, N. Nakamura, T. Shagawa, and M. Hirao, Appl. Phys. Lett. **90**, 191906 (2007).

[21] N. Nakamura, H. Ogi, and M. Hirao, Phys. Rev. B **77**, 245416 (2008).

[22] O. Matsuda, O. B. Wright, D. H. Hurley, V. E. Gusev, and K. Shimizu, Phys. Rev. Lett. **93**, 095501 (2004).

[23] W. Mason, in *Physical Acoustics*, edited by W. Mason (Academic, New York, 1965), Vol. IIIB, p. 254.

[24] See EPAPS Document No. E-PRBMDO-78-047837 for a movie showing the relationship between the strain pulse and the reflectivity change. For more information on EPAPS, see http://www.aip.org/pubservs/epaps.html.

[25] H. G. Tompkins and W. A. McGahan, *Spectroscopic Ellipsometry and Reflectometry* (Wiley, New York, 1999).

[26] L. Ding, T. P. Chen, Y. Liu, C. Y. Ng, and S. Fung, Phys. Rev. B **72**, 125419 (2005).

[27] R. M. A. Azzam and N. M. Basharra, *Ellipsometry and Polarized Light* (North-Holland, Amsterdam, 1977).

[28] P. Etchegoin, J. Kircher, and M. Cardona, Phys. Rev. B **47**, 10292 (1993).

[29] W. F. Love, Phys. Rev. Lett. **31**, 822 (1973).

[30] H. Lin, R. Stoner, H. Maris, and J. Tauc, J. Appl. Phys. **69**, 3816 (1991).

[31] E. Chason, B. W. Sheldon, L. B. Freund, J. A. Floro, and S. J. Hearne, Phys. Rev. Lett. **88**, 156103 (2002).

[32] P. N. Sen and M. F. Thorpe, Phys. Rev. B **15**, 4030 (1977).

[33] F. L. Galeener, Phys. Rev. B **19**, 4292 (1979).

[34] A. E. Geissberger and F. L. Galeener, Phys. Rev. B **28**, 3266 (1983).

[35] R. Vacher and J. Pelous, Phys. Rev. B **14**, 823 (1976).

[36] K. Awazu, S. Ishii, K. Shima, S. Roorda, and J. L. Brebner, Phys. Rev. B **62**, 3689 (2000).

[37] T. Mura, *Micromechanics of Defects in Solids*, 2nd ed. (Martinus Nijhoff, Dordrecht, 1987).

[38] T. Mori and K. Tanaka, Acta Metall. **21**, 571 (1973).

[39] J. D. Eshelby, Proc. R. Soc. London, Ser. A **241**, 376 (1957).

[40] C. F. Ying and R. Truell, J. Appl. Phys. **27**, 1086 (1956).